RSC Advances

ROYAL SOCIETY OF CHEMISTRY

www.rsc.org/advances

RSC Advances

RSCPublishing

ARTICLE

Lithium Chloride Molten Flux Approach to Li_2MnO_3:$LiMO_2$ (M= Mn, Ni, Co) "Composite" Synthesis for Lithium-ion Battery Cathode Applications

Cite this: DOI: 10.1039/x0xx00000x

Received 00th January 2014,
Accepted 00th January 2014

DOI: 10.1039/x0xx00000x

www.rsc.org/

Edwin O. Ortiz-Quiles[a], Jess Soler[b], Mallory Gobet[c], Tetiana Nosach[c], Omar J. García-Ricard[e], Oscar Resto[e], Arturo J. Hernández-Maldonado[e], Steve Greenbaum[d], William C. West[b]* and Carlos R. Cabrera[a]*

In this scientific report, a scalable method for the fabrication of cathodes based on firing pristine compounds Li_2MnO_3 and $LiMn_{0.33}Ni_{0.33}Co_{0.33}O_2$ with lithium chloride molten flux is explored. This approach offers flexibility in synthesis temperature since the process does not require precursor decomposition. Moreover, the synthesis technique allows for the study of the development from the pristine compounds to the final product ($Li_{1.2}Mn_{0.53}Ni_{0.13}Co_{0.13}O_2$). This could help to understand if Li_2MnO_3:$LiMO_2$ material system is a true solid solution or a phase-separated composite. Cathode materials were prepared and characterized by electrochemical charge and discharge studies, electrochemical impedance spectroscopy, and different characterization techniques, including lithium magic angle spinning-nuclear magnetic resonance. Stability studies were conducted to investigate the effects of synthesis duration and temperature on the cathode material. Optimal performance was achieved by firing the pristine compounds for 6 hours at 1000 ºC and for 48 hours at 800 ºC, both in the LiCl molten flux, resulting in a powder with a solid solution behaviour and specific discharge capacity near 240 mAh g^{-1}.

1. Introduction

Lithium ion batteries are commonly used in portable electronic devices such as cellphones and laptops.[1-3] Towards the goal of increasing cell-level specific energy, alternative lithium cathode materials such as those comprising the family of composite or solid solutions of $(x)Li_2MnO_3 + (1-x)LiMO_2$ (M = Mn, Ni, Co) have been extensively studied by many groups.[2-10] These materials offer specific capacities of up to 270 mAh g^{-1}, or even more due to the oxygen in the system.[8] However, commercial use of this promising class of cathode materials has been hindered by several important performance limitations. Among the key demerits of this cathode system, relative to conventional cathodes such as $LiNi_{0.8}Co_{0.2}O_2$, are low life cycle and poor rate capability particularly at reduced temperature.[11]

The typical synthetic route towards preparing this class of compounds has been sol-gel (e.g. dissolving metal acetates in water followed by firing at elevated temperatures of ca. 800 –1000 ºC)[12] or co-precipitation of the metal hydroxides, followed by high temperature co-firing with lithium hydroxide.[13] In both of these approaches, the formation of the desired layered-layered composite oxide necessitates high temperature firing in order to decompose the lithium precursors. Among other methods[14-16], an alternative synthesis route is to prepare Li_2MnO_3–$LiMO_2$ composite oxide cathode materials by firing LiCl molten flux (LCMF) with the pristine compounds Li_2MnO_3 and $LiMO_2$, the latter selected as $LiMn_{0.33}Ni_{0.33}Co_{0.33}O_2$.[8, 17]

LCMF approach has three main advantages. First, the firing temperature is not dictated by the decomposition of any precursor, and the temperature can be varied by simply selecting the appropriate salt flux (e.g. LiI m.p. = 459 ºC, LiCl m.p. = 605 ºC, Li_2SO_4 m.p. = 859 ºC).[18, 19] Lower temperature firings could be explored to reduce the degree of cation disorder towards the goal of improving rate capability. Second, most metals extracted from ores are in their oxide or sulfide form.[20] This method might lead to new synthesis approaches using oxide precursors instead of carbonates or nitrates, which are commonly used for the production of cathodes materials.[3] The third advantage is that this synthetic approach may shed some light on the formation of the $LiMO_2$-type crystallographic system and its electrochemical behavior. While some groups argue that this material system is a true solid solution of Li_2MnO_3 and $LiMO_2$ [10, 21], others have shown evidence that this is a phase-

separated rhombohedral $LiMO_2$ and monoclinic Li_2MnO_3 composite.[22, 23] Given this ambiguity, the LCMF method can provide additional information given that the precursors are mixtures of these two phases. Also, firing at various temperatures in the presence of a molten salt allows the preparation of samples changing the intermixing and possible coalescence of the two species. Furthermore, it could provide a synthetic approach with the benefit of being highly scalable.

In this study, LCMF technique was applied to the pristine rock salt Li_2MnO_3 and layered-layered $LiMO_2$ compounds in an arbitrary 1:1[15] ratio; resulting in a stoichiometrical $Li_{1.2}Mn_{0.53}Ni_{0.13}Co_{0.13}O_2$ cathode material with specific capacity of ca. 240 mAh g^{-1}. This was followed by solid state ^{6,7}Li NMR, which is a powerful tool for probing local structure, dynamics and magnetic phenomena in a wide variety of ordered and disordered materials.[24-28] The interpretation of lithium spectra of battery materials may be complex due to the combination of chemical shift anisotropy (CSA), electric quadrupolar, and paramagnetic interactions.[24] However, higher resolution of the lithium sites may be obtained through the use of magic-angle spinning (MAS).[24,26] The goal of the NMR analysis was to identify the various lithium sites in the synthesized cathode materials prepared from the Li_2MnO_3:$LiMO_2$ (M = Mn, Ni, Co) system, thus offering complementary structural information.

In this work, cathode material of the type $LiMn_aNi_bCo_cO_d$ was prepared by LCMF. Physicochemical characterization provided significant information about the products, including important modifications reached by changing temperature and duration of the synthesis. Further information was obtained from the electrochemical profiles of the synthetized cathode materials.

2. Experimental

2.1 Cathode Preparation

The pristine compound Li_2MnO_3 was prepared by dissolving stoichiometric amounts of lithium acetate dihydrate (Alfa Aesar) and manganese acetate tetrahydrate (Sigma Aldrich) in deionized water, followed by drying while stirring at 120 ºC. The resultant gel was dried on a 300 ºC hotplate; the dry powder was fired successively in room air at 400 ºC, 500 ºC, and again at 500 ºC grinding the powder between each firing step. The powder was then fired for 16 hours in room air at 800 ºC and allowed to cool in the furnace. The other pristine compound, $LiMn_{0.33}Ni_{0.33}Co_{0.33}O_2$ (Quallion), was used as-received.

A 1:1 molar ratio of $LiMn_{0.33}Ni_{0.33}Co_{0.33}O_2$ - Li_2MnO_3 was dispersed in acetone and stirred until the acetone evaporated. LiCl (Aldrich) was then added and manually mixed with the two pristine compounds at approximately twice the mass of the total pristine compound mass, yielding a total mixture mass of 15-20 g. These mixtures were placed in an alumina crucible, fired in a room air furnace at various temperatures and durations described below, and then allowed to furnace cool at the end of the firing. The samples were removed from the furnace, rinsed with deionized water to dissolve the LCMF, filtered, and dried overnight. Following this sequence, a 2 wt% $AlPO_4$ coating was applied to the cathode powder as described in previous works.[29]

To cast the electrodes, a slurry was prepared using 80 wt% active material, 10 wt% poly(vinylene difluoride) (PVDF) (MWavg = 534,000, Sigma Aldrich), and 10 wt% carbon black (Shawinigan) in N-methyl-2-pyrrolidinone (NMP) (Sigma Aldrich). The slurry was aspirated onto an Al foil substrate heated at 140 ºC. Following aspiration, the electrode was vacuum dried overnight at 100 ºC. The coin cells were prepared using CR2032 coin cell hardware with Ni-plated with Al cladding stainless steel cases at the cathode terminal and stainless steel cap, shim, and wave spring at the anode side. Li foil and 1M $LiPF_6$ ethylene carbonate:dimethyl carbonate:diethyl carbonate (EC:DMC:DEC) (1:1:1 vol%, Novolyte Industries) were used as the anode and electrolyte, respectively.

2.2 Physical and electrochemical characterization

X-ray diffraction (XRD) patterns were generated using a Rigaku ULTIMA III with a Cu-Kα (40 kV and 40 mA) radiation source. In situ high temperature XRD measurements were obtained using the same instrument and Rigaku Reactor X module attachment. The latter contains a continuous beryllium window that provides a closed and controlled environment for the sample while allowing passage of X-rays. Upon calibration of the X-ray goniometer, the Reactor X module was attached to the system and analyses were carried out under an air flow of 60 mL/min. Patterns were obtained for 2θ diffraction angles ranging from 2º to 90º at a scanning speed and step size of 3.0º / min and 0.02º, respectively. The Reactor X chamber contents was heated by means of infrared lamp. A thermocouple was embedded into a nickel sample holding plate for temperature reading and control. High-temperature patterns were obtained at 300, 580, 590, 600, 610, 620, and 750 ºC. The final temperature (750 ºC) was held constant and seven sequential XRD patterns were recorded. The tests constituted a total of 3.5 hours of firing time. Prior to heating, an XRD pattern of the precursor and flux mixture was obtained.

Scanning electron microscopy (SEM) and high-resolution transmission electron microscopy (STEM) images were generated using the SEM JSM-7500F - field emission SEM and the HRTEM JEM-2200FS with Cs Corrector - high resolution TEM, respectively.

An Arbin BT2000 battery cycler was used to obtain the electrochemical charge/ discharge cycling results. The cells were charged and discharged for 5 formation cycles within a voltage range of 2.0 – 4.7 V at a rate of C/5, assuming the theoretical capacity was 240 mAh g^{-1}. The charging included a 1 hour current taper step at 4.7 V. Following formation cycling, the cells were cycled at a rate of C/10. An EC-Labs VMP2 potentiostat-galvanostat-frequency response analyzer was used to perform Electrochemical Impedance Spectroscopy (EIS) measurements. Coin cell frequency range was 200 kHz – 50 mHz at an excitation voltage of 5 mV after charged to 4.0 V during the sixth cycle. The data were fitted using ZSimpWin 3.30 assuming a series R(QR)(QR)(CR) equivalent circuit.

Both ^{6}Li and ^{7}Li magic angle spinning nuclear magnetic resonance (MAS NMR) spectroscopy were used in order to obtain detailed information on lithium environments for the pristine and post-fired powdered material samples. Measurements were performed on a Varian-S Direct Drive 300 MHz spectrometer operating at 117.1 MHz and 44.4 MHz for ^{7}Li and ^{6}Li, respectively. ^{7}Li measurements were used to verify certain aspects related to site assignments such as dipolar coupling, but only the ^{6}Li results are discussed here. Powdered samples were packed into 3.2 mm and 1.6 mm zirconia rotors, where the larger volume rotor was practical for the ^{6}Li studies. Spectra were recorded under ambient laboratory conditions and at spinning rates between 17 to 36 kHz. Free-induction decays were obtained using a phase cycled $\pi/2$ pulse – acquire sequence, and echoes were acquired using a typical phase cycled solid-echo pulse sequence ($\pi/2$ pulse – τ – $\pi/2$ pulse – τ – acquire). We used $\pi/2$ pulse widths of 3 μs for ^{7}Li and 4.2 μs for ^{6}Li, and recycle delays of 0.25-1 s in order to avoid signal saturation. The values of τ were chosen such that the signal acquisition was properly synchronized with the spinning rotor (τ = 1/spinning frequency). Depending on the sample, about 10,000 to 50,000 transients were signal-averaged before processing. The spectral frequency scale in the corresponding figures, as given in the normalized units of ppm, is relative to aqueous lithium triflate resonance.

3. Results and discussion

3.1 Physical characterization

3.1.1 X-ray diffraction analysis

XRD patterns indexing for the pristine materials (Figure 1) and products (Figure 2) present diffraction peaks in the 2-theta range from 10 - 70º. Distinctive peaks for a rhombohedral ($R\bar{3}m$), monoclinic ($C_{2/m}$) and face center cubic (fcc) lattices are observed for the $LiMn_{0.33}Ni_{0.33}Co_{0.33}O_2$, Li_2MnO_3 and LiCl, respectively.[18, 22, 30] Frequently, small peaks are observed in the Li_2MnO_3 pattern region between 20 - 25º due to a superlattice cation ordering, which is associated to the $LiMn_6$ in the lattice of transition metal layers.[8, 23, 31] Stoichiometric pseudotrigonal $Li_{1.2}Mn_{0.53}Ni_{0.13}Co_{0.13}O_2$ with the superlattice ordering indexes are present in Figure 2.[30] Substantial differences are not observed between the peaks in Figures 2a, 2b and 2c, with 2 wt% $AlPO_4$ coating, in comparison with Figures 2d and 2e, without 2 wt% $AlPO_4$ coating. This confirms that $AlPO_4$ characteristic peaks are not visible in the XRD patterns. In the case of the samples with and without LCMF, better defined peaks are seen after the LCMF treatment. This may be observed in the (104) peak displayed in Figures 2c and 2e, where peaks are broader and have less definition in the maximum. The calculated $I_{(003)}/I_{(104)}$ ratios for the $AlPO_4$-coated particles after 6 hours/1000 ºC and 48 hour/800 ºC of LCMF were 1.70 and 1.30, respectively. According to this ratio, the synthesis with shorter duration and higher temperature give lower cation intermixing.[22, 32]

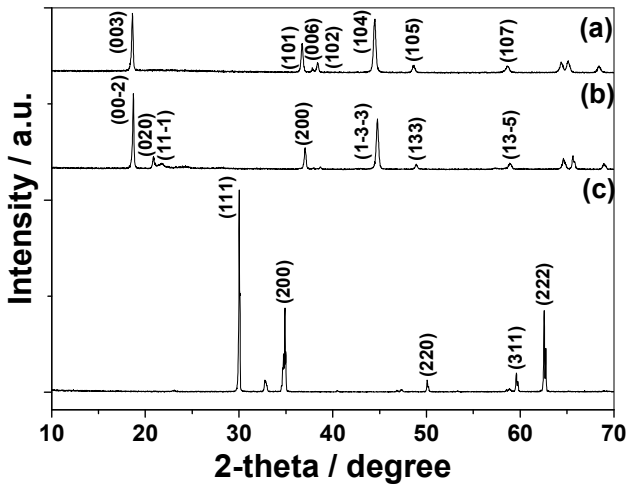

Figure 1. X-ray diffraction patterns of the pristine oxides a) $LiMn_{0.33}Ni_{0.33}Co_{0.33}O_2$, b) Li_2MnO_3 and the c) LiCl salt.

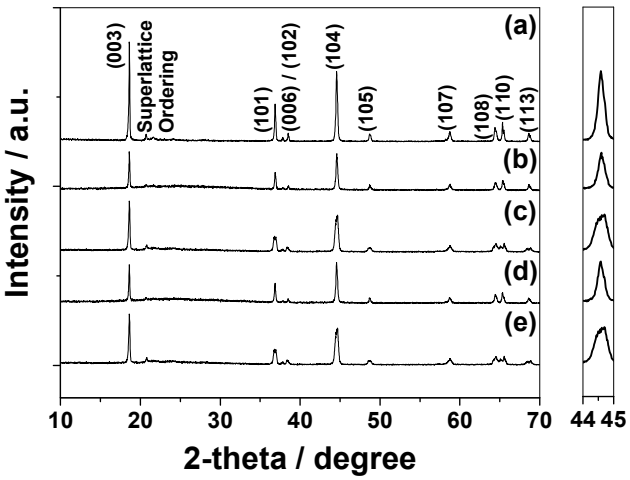

Figure 2. X-ray diffraction patterns of samples of 1:1 (molar basis) Li_2MnO_3:$LiMn_{0.33}Ni_{0.33}Co_{0.33}O_2$ **a)** after firing 6 h/1000 ºC with LCMF, **b)** after firing 48 h/800 ºC with LCMF, **c)** after firing 48 h/800 ºC with no LCMF, **d)** after firing 48 h/800 ºC with LCMF, and **e)** after firing 48 h/800 ºC without LCMF. *Samples **a**, **b** and **c** received a 2 wt% $AlPO_4$ coating post-firing.

A qualitative comparison of the composite oxide layered structure, with minimal cation disorder between the lithium and transition metal sites, show splitting between the (006) and (102) as well as the (108) and (110) diffraction peaks.[22, 33] The two samples of 1:1 Li_2MnO_3:$LiMn_{0.33}Ni_{0.33}Co_{0.33}O_2$, fired without the presence of LCMF (Figures 2c and 2e), reveals less splitting between the (108) and (110) diffraction peaks compared to the samples fired with LCMF (samples 2a, 2b and 2d). This suggests a higher crystallinity quality of the resultant layered-layered metal oxide when fired with the LCMF. The growth in crystallinity is also observed in the crystallite mean size for (104) using Scherrer equation.[34, 35] This gave values, after the coating, of 28 nm, 27 nm and 16 nm for the 6 h/1000 ºC, 48 h/800 ºC with flux, and 48 h/800 ºC without flux, respectively. Moreover, an interplanar spacing of 4.76 Å was

calculated using Bragg's law[36] for these three compounds. This value is similar to the ones observed in the literature using the molten flux synthesis techniques and TEM interplanar spacing analysis.[8] No evident spinel peaks were observed in the XRD patterns.

In situ XRD (Figure 3, top) confirms that LiCl melts, since the LiCl (m.p. = 605 ºC) characteristic peaks disappear at temperatures over 700 ºC. The characteristic peaks of the pristine compounds are still visible at 750 ºC. An examination of the peak near 44º reveals a subtle change in the diffraction pattern as a function of time (Figure 3, bottom). The diffraction pattern recorded at 30 minute intervals for 3.5 hours shows a gradual separation of the two peaks; with a change in the Gaussian peak shape. This may be related to chemical changes by the formation of a secondary phase and/or one or more new planes of diffraction such as (104).

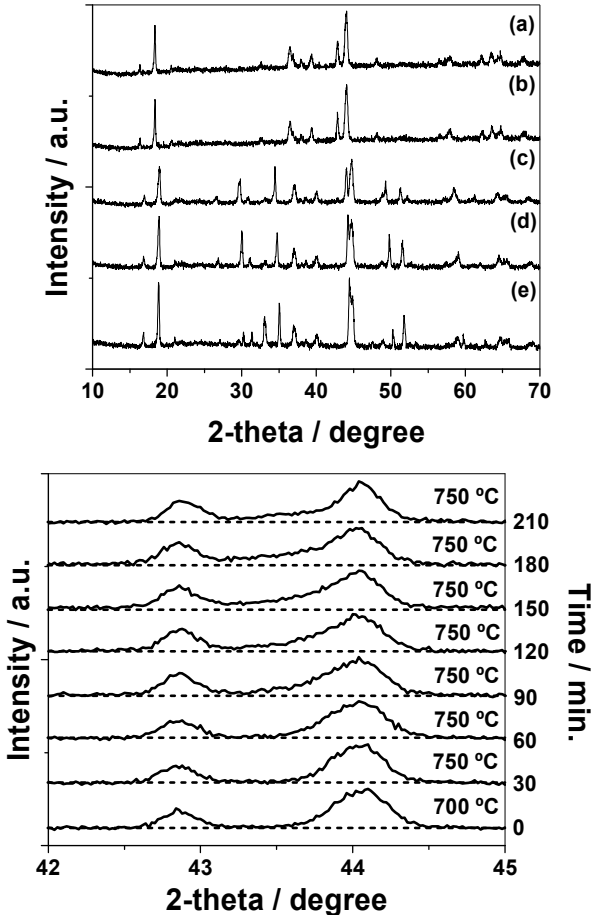

Figure 3. In situ X-ray diffraction patterns of the Li_2MnO_3, $LiMn_{0.33}Ni_{0.33}Co_{0.33}O_2$ and LiCl mixture (top) at 5 different temperatures: **a)** 750 ºC, **b)** 700 ºC, **c)** 600 ºC, **d)** 300 ºC, and **e)** 30 ºC and (bottom) increasing the time to 750 ºC for 3.5 hours.

3.1.2 Electron Microscopy imaging

Surface morphology of the pristine compounds Li_2MnO_3 and $LiMn_{0.33}Ni_{0.33}Co_{0.33}O_2$ are shown in Figures 4a and 4b, respectively. The latter compound generally presents relatively uniform spherical nodules of approximately 1 μm in diameter, with narrow particle size distribution. On the other hand, the former compound presents agglomerates, consisting of smaller primary particles forming larger clusters of ca. 0.3 μm in diameter with a wide secondary particle size distribution. The presence of both of the particle morphologies may be discerned in the post-fired material after 48 h/800 ºC in presence of the LCMF (Figure 4c). For the samples fired at 6 h/1000 ºC (Figure 4d), the agglomerates take a more well-defined octahedral microstructure, without the apparent existence of the pristine structures. Composite systems maintain morphologies similarities with their precursors; this is not the case with the sample treated with the LCMF for 6 h/1000 ºC. STEM-EDS analysis of cathode particles post-firing confirms the expected presence of manganese, cobalt, nickel, and oxygen (Figure 4e), and presence of aluminum and phosphorus associated with the $AlPO_4$ nanoparticle coating applied after the synthesis (Figure 4f).

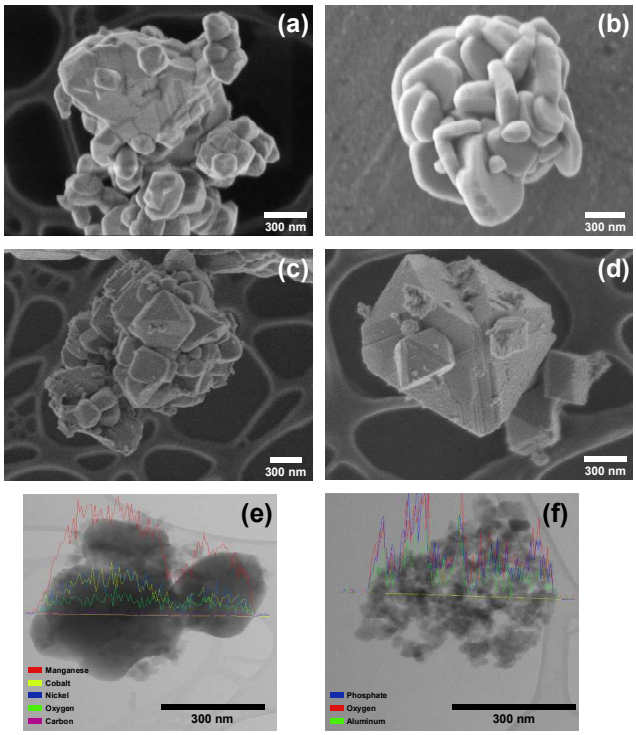

Figure 4. Scanning electron microscopy images of the pristine compounds **a)** Li_2MnO_3 and **b)** $LiMn_{0.33}Ni_{0.33}Co_{0.33}O_2$. and product compounds **c)** $Li_{1.2}Mn_{0.53}Ni_{0.13}Co_{0.13}O_2$ with 2 wt% $AlPO_4$ coating after 48 h/800 ºC in LCMF and **d)** $Li_{1.2}Mn_{0.53}Ni_{0.13}Co_{0.13}O_2$ with 2 wt% $AlPO_4$ coating after 6 h/1000 ºC in LCMF. Scanning transmission electron microscopy and X-ray fluorescence analysis for **e)** $Li_{1.2}Mn_{0.53}Ni_{0.13}Co_{0.13}O_2$ with 2 wt% $AlPO_4$ coating after 48 h/800 ºC in LCMF and f) $AlPO_4$ cluster.

3.2 Li - Nuclear Magnetic Resonances Study

The pristine compound Li_2MnO_3 was studied with ^6Li MAS NMR at various spinning speeds (Figure 5, top). Two characteristic shifts of this structure can be identified and compared to the hyperfine shift scale in accordance to the literature.[26, 27] The shift at 700 ppm is due to lithium sites within the Li layers and the shift at 1400 ppm arises

from lithium sites within the Mn/Li layers. The other peaks in these spectra are spinning sidebands. Close examination of the spectra in Figure 5 (bottom) reveals an incidental temperature dependent shift due to friction between the rotating rotor sleeve (containing the sample) and the surrounding air. This is a well-known Curie-Weiss phenomenon, encountered for paramagnetic materials, and generally results in the observation of more negative shifts with increased spinning rates. The effect, although observed for both environments, is more pronounced for the Mn-layer peak at 1400 ppm. Such effects have been observed in lithium manganese oxides by other groups.[28] Figure 5 (bottom) shows the ^{6}Li spectrum of the $LiMn_{0.33}Ni_{0.33}Co_{0.33}O_2$ pristine compound and the broad isotropic distribution, characteristic of $LiMn_{0.33}Ni_{0.33}Co_{0.33}O_2$ reported by other groups, centered around 500 ppm.[24, 25] The relatively narrow peak at 0 ppm indicates some phase separation, i.e. $LiCoO_2$-like diamagnetic (due to Co^{3+}) environments. The presence of diamagnetic impurities, as the possible source of the 0 ppm signal, may not be ruled out.

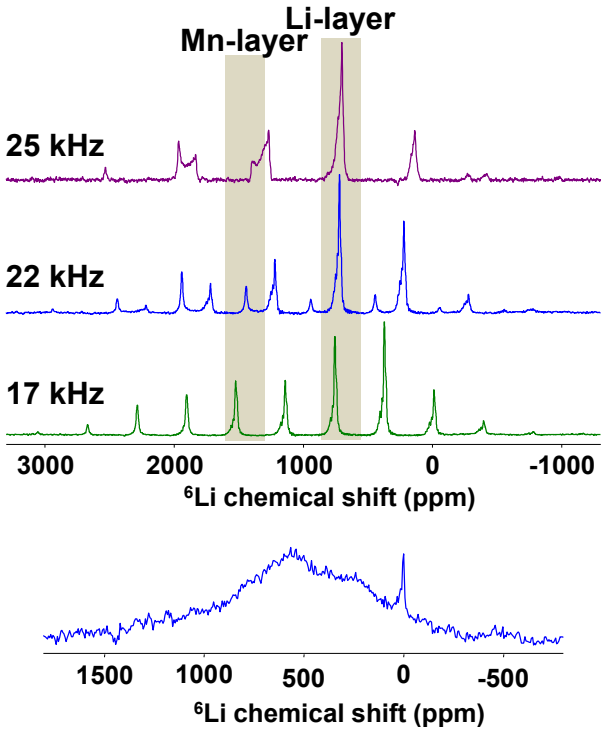

Figure 5. ^{6}Li magic angle spinning NMR spectra of (top) Li_2MnO_3 at spinning speed of 17 kHz, 22 kHz and 25 kHz. The two isotropic shifts represent the two distinct local environments of lithium in the Mn/Li layers and Li layers of Li_2MnO_3. All other peaks are spinning sidebands caused by dipolar coupling. (bottom) $LiMn_{0.33}Ni_{0.33}Co_{0.33}O_2$ acquired at 22 kHz. It consists of a broad signal centered around 500 ppm. The fine peak at 0 ppm is due to an impurity having a Li site diamagnetic environment (e.g. $LiCoO_2$).

In order to understand the effect of LCMF on the Li_2MnO_2–$LiMO_2$ system, ^{6}Li MAS NMR spectra was collected at 23 kHz for the sample without LCMF and two other samples that were co-fired with molten salt for 48 h/800 ºC and 6 h/1000 ºC (Figure 6). The spectrum for the untreated sample shows three isotropic shifts at 0 ppm, 700 ppm and 1400 ppm. As explained above, these isotropic peaks were observed in the pristine compounds and represent lithium in diamagnetic phase ($LiCoO_2$-like lithium environment), Li- and Mn-layered environments, respectively. Because of different NMR sensitivities due perhaps to different spin-spin relaxation times of the pristine compounds, the $LiMO_2$ phase does not appear clearly in this spectrum. In addition to these 3 sites, a new site around 500 ppm is observed after LiCl treatment. This new site is different in appearance from the broad site distribution present in the pristine $LiMO_2$. As mentioned before, the spinning sidebands in the MAS-NMR provide information of the coordination symmetry for lithium environments. Figure 6 shows that for the isotropic shift at 1400 ppm the side-band manifold (marked as '*') is distributed asymmetrically. This confirms that the pattern is governed by the chemical shift interaction with anisotropy and used to describe the coupling between Li and Mn ions in the Mn layer site. On the other hand, the side-band manifolds for resonances at 700 ppm and 500 ppm (marked as '0' and '=' respectively) represent different geometric arrangements around Li ions and have a more symmetrical shape, in part because the Li-Mn distances are larger and ions are arranged more symmetrically around the Li-layer site. A smaller dipolar coupling like this can be used as a signature for the tetrahedral site in these compounds. These assignments were confirmed by ^{7}Li results. Additionally to the new 500 ppm site, the 700 ppm site is much broader in the LiCl treated sample than in the untreated one, indicating a correspondingly broad distribution of environments. In fact, the integrated intensity in this region is rather larger than in the untreated material. These general features are observed even in the 48 h/800 ºC LiCl fired sample, but are clearly more apparent in the 6 h/1000 ºC material.

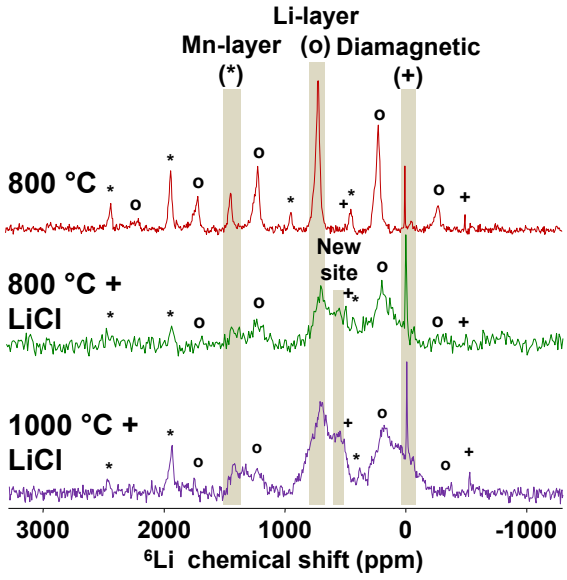

Figure 6. ^{6}Li magic angle spinning NMR spectra of the Li_2MnO_3:$LiMn_{0.33}Ni_{0.33}Co_{0.33}O_2$ at 23 kHz a) after firing 48 h/800 ºC with no LCMF, b) after firing 48 h/800 ºC with LCMF, c) after firing 6 h/1000 ºC with LCMF.

^{6}Li MAS NMR with different spinning speeds were performed (Figure 7) to identify the supplementary site of the $Li_{1.2}Mn_{0.53}Ni_{0.13}Co_{0.13}O_2$. For the spinning speed of 17 kHz it is difficult to see all the resonances in ^{6}Li spectrum and some of the weaker peaks are obscured due to the overlapping of the sidebands originated from the more intense resonances. Higher spinning speed gives a higher resolution of the NMR spectra and new peaks can be identified, such as the peak at 500 ppm. Figure 7 illustrates the broad distribution from 0 to 1000 ppm, which can be related to the presence of the disordered chemical environment in the Li layer sites.

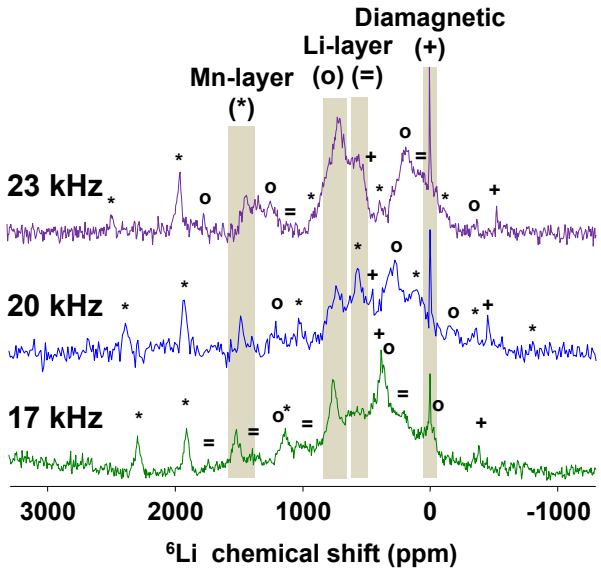

Figure 7. Comparison of the ^{6}Li magic angle spinning NMR spectra of the Li_2MnO_3:$LiMn_{0.33}Ni_{0.33}Co_{0.33}O_2$ after firing 6 h/1000 ºC with LCMF at 17 kHz, 22 kHz and 25 kHz spinning speeds. Higher spinning speed of 20 kHz and 23 kHz give a better resolution to the NMR spectra and new peak at 500 ppm can be identified.

NMR studies confirm that Li resides in two sites for the Li_2MnO_3 (in the Li-and Mn-layer sites) and one location broadly distributed Li-layered configuration for the $LiMn_{0.33}Ni_{0.33}Co_{0.33}O_2$ as previously reported in the literature.[25, 37] Following the molten LiCl synthesis, the lithium environment in the post-fired material clearly becomes more disordered. Towards the debate of whether the Li_2MnO_3–$LiMO_2$ system is a phase separated composite or true solid solution of the pristine compounds, the NMR data strongly suggests the latter case, given that phase separated composites should likely retain the similar Li environment of the pristine compounds, which is contrary to the post-firing NMR data herein. Rather, the disordered Li environment is likely due to diffusion of Li into its sites as is known to exist for $Li_{1.2}Mn_{0.53}Ni_{0.13}Co_{0.13}O_2$ assuming stoichiometric product. LCMF may facilitate the Li_2MnO_3 domains-like to occur in the layered oxide material.

3.2 Electrochemical characterization

3.2.1 Charge and discharge capacity

Electrochemical capacity measurements were completed to coated cathode powders from 2.0 V to 4.7 V. Figure 8 shows the first C/5 assuming a theoretical specific capacity of 240 mAh g^{-1} charge and discharge capacity of three half cells. The images presented in 8a, 8b, and 8c are for the cathode materials prepared by firing the pristine compounds with the LCMF at two different conditions (Figures 8a and 8b) and without applying LCMF treatment (Figure 8c). The specific charge and discharge capacities ware 112 mAh g^{-1} and 96 mAh g^{-1}, respectively, for the system fired at 48 h/800 ºC without the LCMF (Figure 8c). An abnormal behaviour is observed at the beginning of the charging process in the region under 4.4 V, associated to difficulties to complete the process of Li-extraction and Ni^{2+} oxidation to Ni^{4+}. Other studies suggest the possibility of Ni^{2+} interfering with the Li-extraction process.[32, 38-40] In addition, this region is associated to structural changes in the Li_2MnO_3-like region with its so-called oxygen release plateau expected at 4.5 V vs. Li/Li^+, and with the solid electrolyte interphase (SEI) formation.[8, 21, 41]

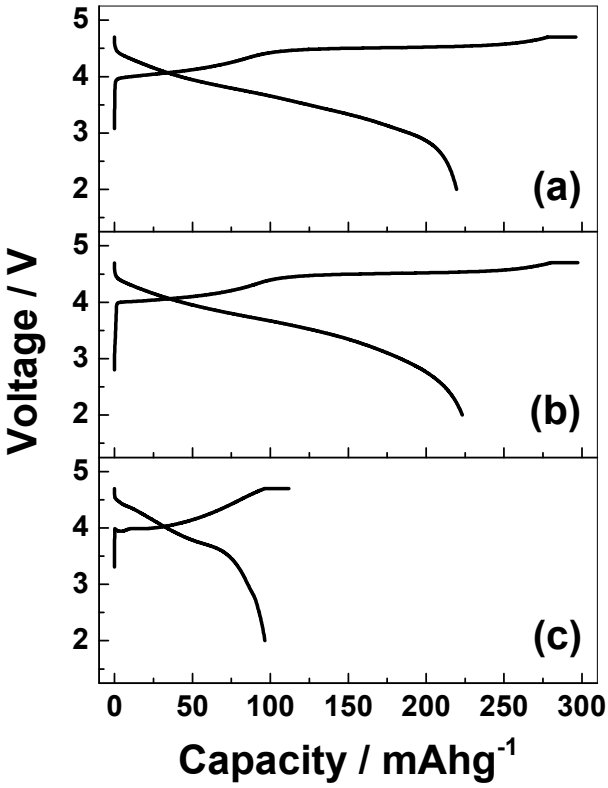

Figure 8. First charge and discharge at C/5 rate of a coin cell with a cathode active material consisting of 1:1 Li_2MnO_3:$LiMn_{0.33}Ni_{0.33}Co_{0.33}O_2$ prepared by firing the pristine compounds with a LCMF by **a)** 6 h/1000 ºC and **b)** 48 h/800 ºC, and **c)** without the LiCl flux at 48 h/ 800 ºC. Samples include a post-firing 2 wt% $AlPO_4$ coating.

In contrast, Figure 8a and 8b show the first charge and discharge of two coin cells with the pristine compounds fired at 6 h/1000 ºC and 48 h/800 ºC with the molten LCMF. The specific charge and discharge capacities for 6 h/1000 ºC were 296 mAh g^{-1} and 220 mAh g^{-1}; and for 48 h/800 ºC were 295 mAh g^{-1} and 228 mAh g^{-1},

respectively. In these cases, usually well resolved charge plateau were observed at about 4.5 V in both of them with an irreversible capacity loss of approximately 70 mAh g^{-1} similar to the ones in the literature.[8]

Four coin cells prepared at 48 h/800 ºC and additional four prepared at 6 h/1000 ºC, all of them after the LCMF treatment, were tested at C/5 rates through five cycles and the average specific capacity is shown in Figure 9. The electrochemical profiles of four coin cells, two of each condition, were further tested at C/10 for 30 more cycles (Figure 10) displaying satisfactory cycling stability. As expected, higher temperatures appear to reduce the time needed to complete the reaction and reach the maximum specific capacity.

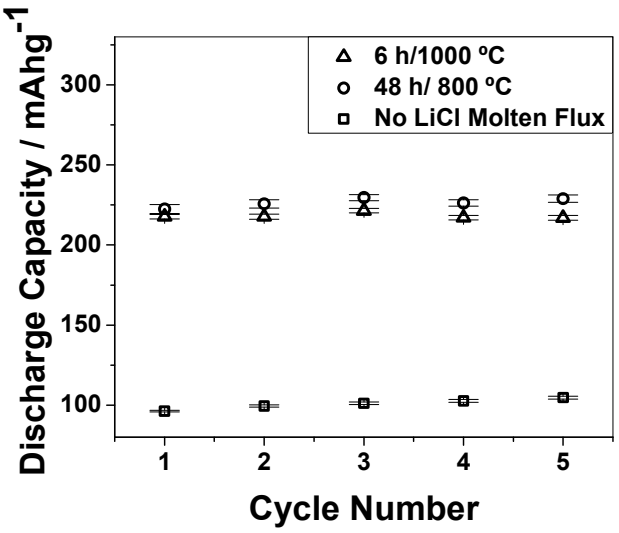

Figure 9. Average specific discharge capacity for 4 coin cells per experimental condition at C/5 (top) for 5 cycles as a function of firing duration. The averages are based on 4 cells at 48 h/800 ºC and 6 h/1000 ºC with LCMF, and 48 h/800 ºC without the LCMF.

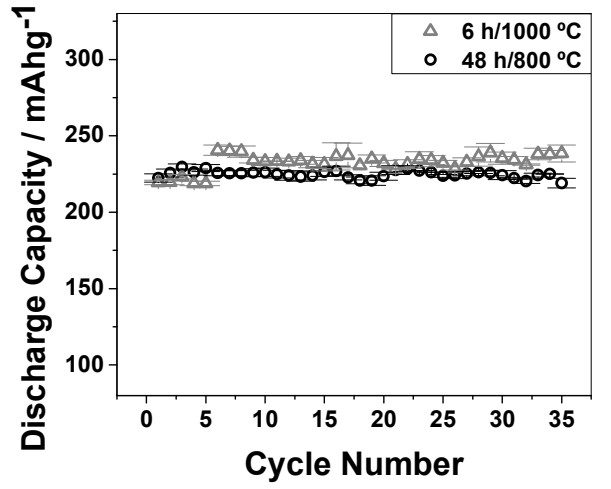

Figure 10. Average discharge capacities for three coin cells per experimental conditions using cathodes with the pristine compounds fired with the LCMF for 48 h/800 ºC and 6 h/1000 ºC.

LiCl treatment can provide higher specific capacities in comparison to the system without it. Firing at 6 h/1000 ºC with LCMF results in a cathode material with slightly higher specific discharge capacity relative to cathode material fired at 48 h/800 ºC with LCMF. Even with different morphologies, as appreciated in the SEM images, similar electrochemical results were achieved. Changes after employing LCMF are consistent with the XRD data, suggesting crystal structure variations, and the NMR results, indicating a vastly altered Li site population characteristic of the Li layer for materials fired in the presence of the melted salt. [10, 24, 42]

3.2.2 Electrochemical Impedance Spectroscopy (EIS)

Figure 11 presents the complex plane or Nyquist plot of three coin cells, one (Figure 11a) prepared with a cathode powder made with the pristine compounds fired with the LCMF at 6 h/1000 ºC, other (Figure 11b) with the pristine compounds fired in LCMF at 48 h/800 ºC, and the third one (Figure 11c) fired without the LCMF at 48 h/800 ºC. As in the case of the charge and discharge capacity studies, all coin cells cathode materials were previously coated for the EIS studies. These three figures show the EIS profile for the cells at five different temperatures. As can be observed from the figures, the total resistance is approximately inversely proportional to the temperature. However, this effect is considerably reduced when the cathode powders are synthesized with the LiCl treatment. This is more obvious in the 48 h/800ºC. At lower frequencies, appears a curve that could be related to diffusion or charge transfer processes. Recently studies suggest the second, charge transfer, as the process occurring during mHz frequencies.[8, 10, 42] This implies the diffusion element appearing in even lower frequencies, probably at the μHz range. It is possible that diffusion and charge transfer are both affecting the system during mHz

A fitted curve example using ZSimpWin 3.30, and the equivalent circuit without the Warburg diffusion element are presented in Figure 12 (top). Four main resistances had been confirmed: resistances of the electrolyte (R_e), two more resistances related to the Li^+ migration through the SEI (R_{S1} and R_{S2}), and the last one related to the charge transfer between the film and the solution (R_{CT}).[10, 42] A constant phase element was employed instead of a capacitor for R_{S1} and R_{S2} searching for better results in the simulation. Mainly, because the Li^+ migration can be interrupted and possible phase changes can occurs.[43] These constant phase elements were mathematically transformed to capacitors by the impedance application, to obtain the final resistance value. R_{S1} and R_{S2} are hard to differentiate in the coin cells without the LCMF. This may be correlated to the abnormal behaviour of the coin cells without the LCMF observed in the first charge and discharge process. Furthermore, even after the transformation, R_{CT} could not be determined at temperature near -20 ºC. All others resistances were reduced after the LCMF, specially R_{S2} and R_{CT} which contain resistance values with higher magnitude frequencies.

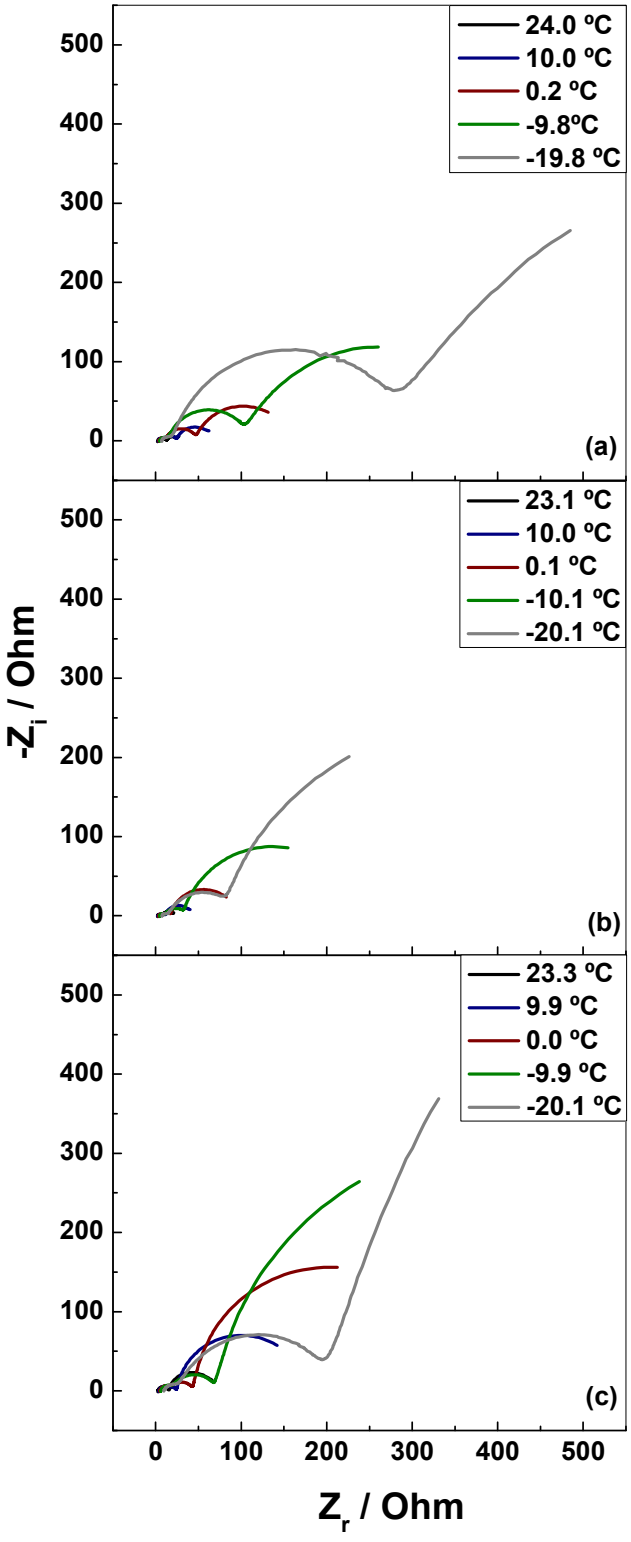

Figure 11. EIS data of a cell incorporating a cathode with active material consisting of 1:1 Li_2MnO_3–$LiMn_{0.33}Ni_{0.33}Co_{0.33}O_2$ prepared by firing the pristine compounds **a)** with LCMF for 6 h/1000 ºC, **b)** with LCMF for 48 h/800 ºC and **c)** without the LCMF for 48 h/800 ºC.

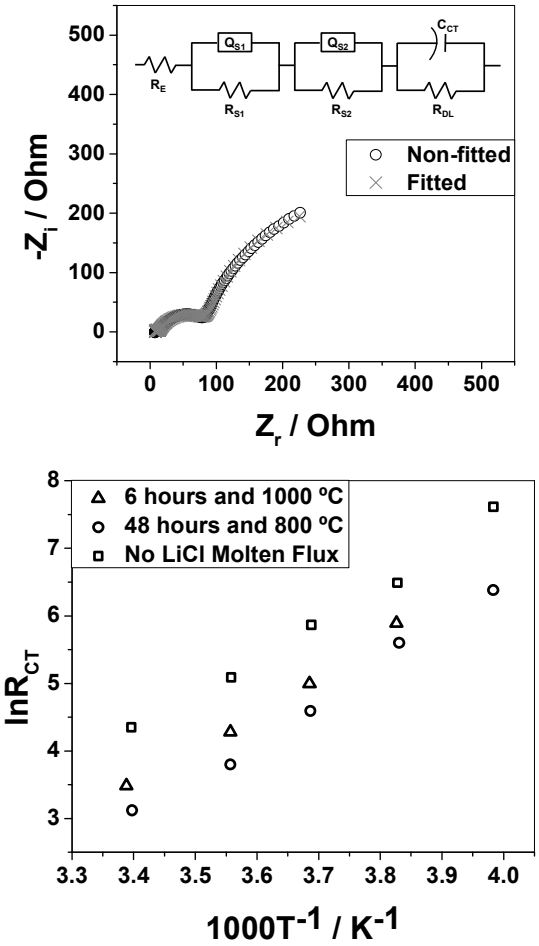

Figure 12. (Top) Equivalent circuit used for the fitting and the EIS complex plot with the raw impedance versus the fitted curve obtained from a battery with a cathode powder with the LCMF for 48 h/800 ºC EIS analysis at 20 ºC. (Bottom) Arrhenius plots for R_{CT} for three synthetic conditions.

Resistance values were correlated with temperature, plotted and the Activation Energy (E_a) was calculated using Arrhenius equation from the plots slopes.[44, 45] Figure 12 (bottom) shows R_{CT} as one example of these plots; and Table 1 summarizes the results for all the resistances and its E_a. Even after using the $AlPO_4$ coating, the activations energies still remain high. Moreover, these two resistances (R3 and R4) are more affected by temperature changes, which suggest that the Li^+ migration and charge transfer processes are important in determining the practical specific capacity of the cathode. After the co-firing process with and without LCMF, the activation energy varies in all resistances, and is lower for R_E after the flux treatment. In the case of R_{S2}, the E_a changed drastically, where the E_a value is higher for the system where the flux was employed. Surprisely, from the SEM images, a better organized system is observed for the sample prepared at 6 h/1000 ºC. Li-NMR results confirmed changes on the Li^+ environment. Moreover, the R_{CT} is slightly lower for the 6 h/1000 ºC, probably do to a better surface organized system, as well.

Conditions	Activation Energy (E_a / kJmol^{-1})			
	R_E	R_{S1}	R_{S2}	R_{CT}
6 hours and 1000 ºC	14	13	41	46
48 hours and 800 ºC	15	9	41	48
No LiCl Molten Flux	16	12	36	46

Table 1. Activation Energies for three synthetic conditions.

4. Conclusion:

A scalable approach for the fabrication of the layered-layered composite oxide $Li_{1.2}Mn_{0.53}Ni_{0.13}Co_{0.13}O_2$ has been demonstrated and optimum conditions for superior electrochemical properties were investigated. XRD and electron microscopy divulge a higher crystallinity in the system after the LCMF. The NMR data strongly suggests that the post-fired Li_2MnO_3:$LiMO_2$ forms a true solid solution rather than a phase separated composite, given that the latter should likely retain the similar Li environment of the pristine compounds, which is contrary to the post-firing NMR data. Rather, the disordered Li environment is likely due to the diffusion of Li^+ into its sites as is known to exist for the final product of $Li_{1.2}Mn_{0.53}Ni_{0.13}Co_{0.13}O_2$. Electrochemical studies revealed an improvement in the discharge capacity and cycle stability after the LCMF procedure. A high specific capacity ca. 230 mAh g^{-1} has been achieved at C/5 and C/10. According to the EIS studies, the system appears to be highly controlled by the charge transfer phenomena and the resistances of the system are affected by the LCMF treatment. This includes a reduction on the resistance to charge transfer values at lower working temperature for the coin cells tested within cathode material treated with the LCMF. As possible mechanism for the LCMF treatment, longer treatment time may enhance the mobility of Li^+ through the oxides, reorganizing this cation to facilitate its movement across the material. On the other hand, higher temperatures may increase the interlayer distances of the system facilitating the mixing of the layered material with the rock salt. Prolonged overtreatment synthesis at high temperature may adversely affect the cathode material performance, as presented in the supporting information.

5. Acknowledgements

This work was carried out at the University of Puerto Rico and at Jet Propulsion Laboratory, California Institute of Technology, under contract with the National Aeronautics and Space Administration within the NASA Office of Chief Technologist. The project was partially funded by NASA-URC Grant Number NNX10AQ17A. NMR measurements at Hunter College were supported by Grant # DE-SC0005029 from the Basic Energy Sciences Division of the U.S. Department of Energy.

6. Notes and References

6.1 Addresses

[a]Department of Chemistry, University of Puerto Rico - Rio Piedras Campus, San Juan, PR 00936

[b]Jet Propulsion Laboratory, California Institute of Technology, Pasadena, CA 91109

[c]Hunter College of City University of New York, New York, NY 10065

[d]Department of Chemical Engineering, University of Puerto Rico at Mayagüez, Mayagüez, PR 00681-9000

[e]Department of Physics, University of Puerto Rico-Rio Piedras Campus, San Juan, PR 00936

*Corresponding authors, Emails: william.c.west@jpl.nasa.gov, carlos.cabrera2@upr.edu

6.2 References

1. Y.-M. Chiang, *Science*, 2010, **330**, 1485-1486.
2. M. M. Thackeray, C. Wolvertonb and E. D. Isaacsc, *Energy Environ. Sci.*, 2012, **5**, 7854-7863.
3. M. S. Whittingham, *Chem. Rev.*, 2004, **104**, 4271-4301.
4. W. C. West, J. Soler, M. C. Smart, B. V. Ratnakumar, S. Firdosy, V. Ravi, M. S. Anderson, J. Hrbacek, E. S. Lee and A. Manthiram, *J. Electrochem. Soc.*, 2011, **158**, A883-A889.
5. M. Mohamedi, M. Makino, K. Dokko, T. Itoh and I. Uchida, *Electrochim. Acta*, 2002, **48**, 79-84.
6. H. Yu, H. Kim, Y. Wang, P. He, D. Asakura, Y. Nakamura and H. Zhou, *Phys. Chem. Chem. Phys.*, 2012, **14**, 6584-6595.
7. V. Pralong, *Prog. Solid State Chem.*, 2009, **37**, 262-277.
8. S. J. Shi, J. P. Tu, Y. Y. Tang, X. Y. Liu, X. Y. Zhao, X. L. Wang and C. D. Gu, *J. Power Sources*, 2013, **241**, 186-195.
9. F. Amalraj, M. Talianker, B. Markovsky, D. Sharon, L. Burlaka, G. Shafir, E. Zinigrad, O. Haik, D. Aurbach, J. Lampert, M. Schulz-Dobrick and A. Garsuchc, *J. Electrochem. Soc.*, 2013, **160**, A324-A337.
10. H. Yu and H. Zhou, *J. Phys. Chem. Lett.*, 2013, 1268-1280.
11. S. S. Zhang, K. Xu and T. R. Jow, *J. Power Sources* 2003, **115**, 137-140.
12. W. C. West, J. Soler and B. V. Ratnakumar, *J. Power Sources* 2012, **204**.
13. R. Li, F. Gong, H. Lin and W. Wang, *Ionics*, 2005, **11**, 343-351.
14. X. Wei, S. Zhang, L. He, G. Liu and P. Yang, *Int. J. Electrochem. Sci.*, 2013, **8**, 1885-1894.
15. J. Bareño, M. Balasubramanian, S. H. Kang, J. G. Wen, C. H. Lei, S. V. Pol, I. Petrov and D. P. Abraham, *Chem. Mater.*, 2011, **23**, 2039-2050.
16. N. Balke, S. Jesse, A. N. Morozovska, E. Eliseev, D. W. Chung, Y. Kim, L. Adamczyk, R. E. García, N. Dudney and S. V. Kalinin, *Nat. Nanotechnol.*, 2010, **5**, 749-754.
17. W. Tang, H. Kanoh and K. Ooi, *Electrochem. Solid-State Lett.*, 1998, **1**, 145-146.
18. H. E. Swanson, H. F. McMurdie and M. C. Morris, *Standard X-ray Diffraction Powder Patterns*, The National Bureau of Standards, Washington, D.C., 1968.
19. G. J. Janz and C. G. M. Dijkhuis, *NIST Molten Salts*, NSRDS, Washington, 1969.
20. A. Vignes, in *Extractive Metallurgy 1: Basic Thermodynamics and Kinetics*, ed. A. Vignes, ISTE Ltd and John Wiley & Sons, Inc. , Great Britain United States, 2011, pp. 41 - 72.
21. Z. Q. Deng and A. Manthiram, *J. Phys. Chem. C*, 2011, **115**, 7079-7103.
22. C. Ghanty, R. N. Basu and S. B. Majumdera, *J. Electrochem. Soc.*, 2012, **159**, A1125-A1134.
23. J. Gim, J. Song, H. Park, J. Kang, K. Kim, V. Mathew and J. Kim, *Nanoscale Res. Lett.*, 2012, **7**, 60-69.
24. W.-S. Yoona, N. Kima, X.-Q. Yang, J. McBreen and C. P. Greya, *J. Power Sources*, 2003, 649-653.
25. D. Zeng, J. Cabana, J. Bréger, W.-S. Yoon and C. P. Grey, *Chem. Mater.*, 2007, **19**, 6277–6289.
26. C. P. Grey and Y. J. Lee, *Solid State Sci.*, 2003, **5**, 883-894.
27. C. P. Grey and N. Dupre, *Chem. Rev.*, 2004, **104**, 4493-4512.
28. B. Gee, C. R. Horne, E. J. Cairns and J. A. Reimer, *J. Phys. Chem. B*, 1998, **102**, 10142-10149.

29. W. C. West, J. Soler and B. V. Ratnakumar, *J. Power Sources*, 2012, **204**, 200-204.
30. M. M. Thackeray, S.-H. Kang, C. S. Johnson, J. T. Vaughey, R. Benedeka and S. A. Hackney, *J. Mater. Chem.*, 2007, **17**, 3112-3125.
31. Y. Wu, A. V. Murugan and A. Manthiram, *J. Electrochem. Soc.*, 2008, **155**, A635-A641.
32. C. Yu, G. Li, X. Guan, J. Zheng, D. Luob and L. Li, *Phys. Chem. Chem. Phys.*, 2012, **14**, 12368-12377.
33. Y.-K. Sun, H.-B. Kang, S.-T. Myung and J. Prakashd, *J. Electrochem. Soc.*, 2010, **157**, A1335-A1340.
34. M. Y. Son, J. H. Kim and Y. C. Kang, *Int. J. Electrochem. Sci.*, 2013, **8**, 2417-2429.
35. R. E. Dinnebier and S. J. L. Dillinge, *Powder Diffraction: Theory and Practice*, The Royal Society of Chemistry, United Kindom, 2008.
36. A. Alemi, S. Khademinia, S. W. Joo, M. Dolatyari and A. Bakhtiari, *Int. Nano Lett.*, 2013, **3**, 1-11.
37. B. Xu, C. R. Fell, M. Chic and Y. S. Meng, *Energy Environ. Sci.*, 2011, **4**, 2223-2233.
38. M. Gu, I. Belharouak, A. Genc, Z. Wang, D. Wang, K. Amine, F. Gao, G. Zhou, S. Thevuthasan, D. R. Baer, J.-G. Zhang, N. D. Browning, J. Liu and C. Wang, *Nano Lett.*, 2012, **12**, 5186−5191.
39. K. Kang, Y. S. Meng, J. Bréger, C. P. Grey and G. Ceder, *Science*, 2006, **311**, 977-980.
40. A. Watanabe, F. Matsumoto, M. Fukunishi, G. Kobayashi, A. Ito, M. Hatano, Y. Ohsawa and Y. Sato, *J Electrochem Soc Jp*, 2011, **80**, 561-565.
41. S.-H. Kang and M. M. Thackeray, *Electrochem. Commun.*, 2009, **11**, 748-751.
42. Q.-C. Zhuang, X.-Y. Qiu, S.-D. Xu, Y.-H. Qiang and S.-G. Sun, in *Lithium Ion Batteries - New Developments*, ed. I. Belharouak, InTech, 2012, pp. 189-224.
43. J. Bisquert, G. Garcia-Belmonte, P. Bueno, E. Longo and L. O. S. Bulhões, *J. Electroanal. Chem.*, 1998, **452**, 229-234.
44. P. Rosaiah and O. M. Hussain, *Adv. Mat. Lett.*, 2013, **4**, 288-295.
45. H. Yu, Y. Wang, D. Asakura, E. Hosono, T. Zhang and H. Zhou, *RSC Adv.*, 2012, **2**, 8797-8807.

Electronic Supplementary Information (ESI) available: [Two documents with Charge/Discharge and the EIS Data Summary]. See DOI: 10.1039/b000000x/

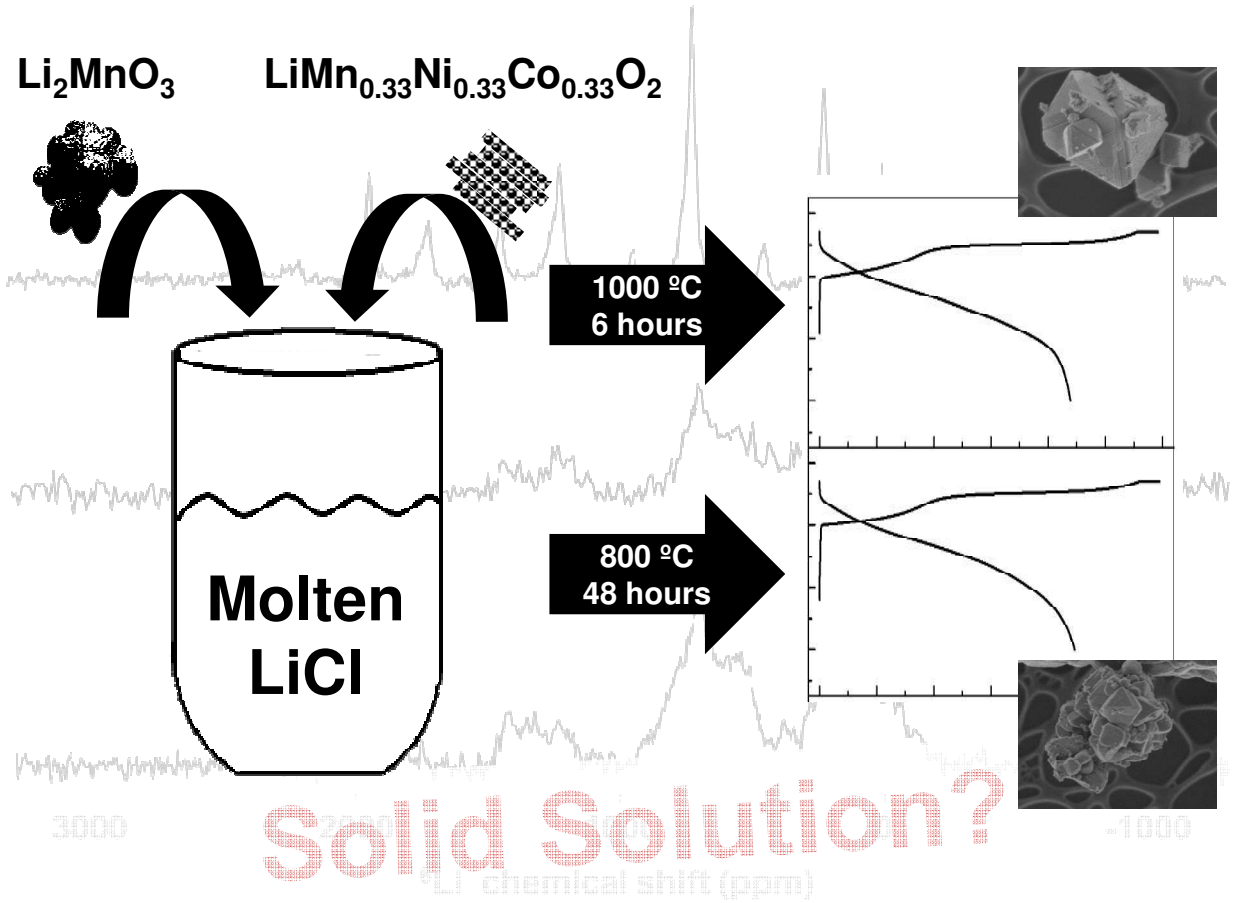

GRAPHICAL ABSTRACT